On Measuring the Terms of the Turbulent Kinetic Energy Budget from an AUV

LOUIS GOODMAN

School for Marine Science and Technology, University of Massachusetts—Dartmouth, New Bedford, Massachusetts

EDWARD R. LEVINE

Autonomous Systems and Technology Department, Naval Undersea Warfare Center, Newport, Rhode Island

ROLF G. LUECK

School of Earth and Ocean Sciences, University of Victoria, Victoria, British Columbia, Canada

(Manuscript received 28 September 2005, in final form 5 December 2005)

ABSTRACT

The terms of the steady-state, homogeneous turbulent kinetic energy budgets are obtained from measurements of turbulence and fine structure from the small autonomous underwater vehicle (AUV) Remote Environmental Measuring Units (REMUS). The transverse component of Reynolds stress and the vertical flux of heat are obtained from the correlation of vertical and transverse horizontal velocity, and the correlation of vertical velocity and temperature fluctuations, respectively. The data were obtained using a turbulence package, with two shear probes, a fast-response thermistor, and three accelerometers. To obtain the vector horizontal Reynolds stress, a generalized eddy viscosity formulation is invoked. This allows the downstream component of the Reynolds stress to be related to the transverse component by the direction of the finescale vector vertical shear. The Reynolds stress and the vector vertical shear then allow an estimate of the rate of production of turbulent kinetic energy (TKE). Heat flux is obtained by correlating the vertical velocity with temperature fluctuations obtained from the FP-07 thermistor. The buoyancy flux term is estimated from the vertical flux of heat with the assumption of a constant temperature–salinity (T–S) relationship. Turbulent dissipation is obtained directly from the usage of shear probes.

A multivariate correction procedure is developed to remove vehicle motion and vibration contamination from the estimates of the TKE terms. A technique is also developed to estimate the statistical uncertainty of using this estimation technique for the TKE budget terms. Within the statistical uncertainty of the estimates herein, the TKE budget on average closes for measurements taken in the weakly stratified waters at the entrance to Long Island Sound. In the strongly stratified waters of Narragansett Bay, the TKE budget closes when the buoyancy Reynolds number exceeds 20, an indicator and threshold for the initiation of turbulence in stratified conditions. A discussion is made regarding the role of the turbulent kinetic energy length scale relative to the length of the AUV in obtaining these estimates, and in the TKE budget closure.

1. Introduction

Although oceanographers have had a long history of interest in turbulent mixing, both for the parameterization of subgrid-scale processes in ocean numerical models, as well as for the study of the processes themselves, direct measurements of turbulent mixing are very limited. The methods currently used to study ocean turbulent mixing are mostly indirect. For example, the vertical flux (or mixing) of momentum is obtained from measurements of the rate of dissipation of kinetic energy ε and the finescale vertical shear. The vertical fluxes of heat and buoyancy are usually obtained with some version of the Osborn (1980) formulation and the assumption of a constant mixing efficiency $\Gamma = 0.2$. In the past two decades, there have been increased efforts in the laboratory (Ivy et al. 1998; Itsweire et al. 1986; Stillinger et al. 1983) as well as in the field (Moum 1990; Fleury and Lueck 1994; Wolk and Lueck 2001) to obtain, directly and simultaneously, the fluxes of momen-

Corresponding author address: Louis Goodman, School for Marine Science and Technology, University of Massachusetts—Dartmouth, 706 South Rodney French Boulevard, New Bedford, MA 02744-1221.
E-mail: lgoodman@umassd.edu

tum and heat without recourse to invoke some specific value for the mixing efficiency. However, for the case of stratified turbulence, the direct estimates of the mixing efficiency are frequently close to 0.2, which lends credence to the method of Osborn. Turbulent mixing has been the subject of many reviews (i.e., Gregg 1987; Gargett 1989; Caldwell and Moum 1995).

For the past 30 yr, the standard technique of measuring turbulent quantities in the ocean has been with vertical microstructure profilers—a technique pioneered by Cox et al. (1969), Osborn (1974), and Gregg et al. (1982). These techniques provide a very high-resolution vertical distribution of turbulent quantities. More recently, with the advent of rapid loosely tethered profilers, some horizontal information on the distribution of the turbulent quantities can also be inferred. Efforts are presently underway to obtain both fixed-point time series and horizontal sampling of turbulent quantities. A very extensive review of oceanic turbulence measurement techniques is provided in the special issue of the *Journal of Atmospheric and Oceanic Technology* (1999, Vol. 16, No. 11) and by Lueck et al. (2002).

Horizontal transects of turbulence can resolve structures on scales that are not resolvable with vertical profiling (Yamazaki et al. 1990). In the past, horizontal sampling, using towed bodies and submarines, has provided unique views of internal waves (Gargett 1982), salt fingers (Fleury and Lueck 1992), and turbulence (Osborn and Lueck 1985). Vibration measurements taken aboard the Naval Undersea Warfare Center (NUWC) Large Diameter Unmanned Underwater Vehicle (LDUUV), in Narragansett Bay (Levine and Lueck 1999), indicated that this platform was sufficiently stable to obtain horizontal measurements of the dissipation rate in shallow water. Following this, Levine et al. (2000) demonstrated that a small autonomous underwater vehicle (AUV) can also be used to measure the turbulent dissipation rate.

In this manuscript, we examine whether a small AUV can be used to directly estimate the turbulent fluxes of momentum and heat using standard fine- and microstructure sensors. The effects of body motion and probe vibration on these estimates are minimized by usage of a coherent subtraction technique using all three components of accelerometer measurements. To assess the uncertainty of these estimates, a numerical statistical procedure for their uncertainty is developed. We also examine whether these flux estimates, along with our estimate of the dissipation rate, result in the closure of the steady and homogeneous turbulence kinetic energy (TKE) budget. Closure of the TKE budget has been an important assumption made in the standard technique of estimating eddy viscosities and diffusivities from the estimate of turbulent dissipation rate (Gregg 1987).

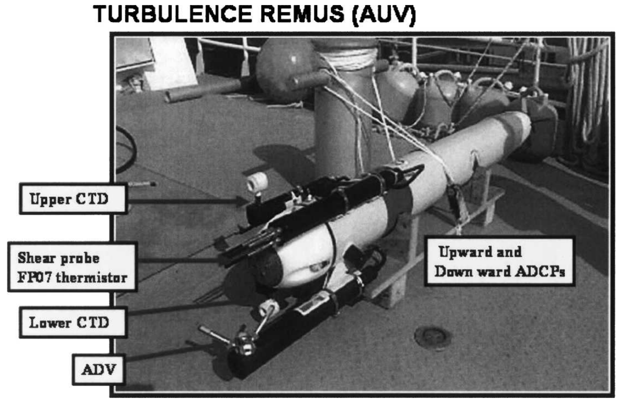

FIG. 1. The REMUS AUV and its main external sensors.

Two different datasets are examined. One is from measurements taken in a strongly stratified tidal channel during summer, and the other from measurements collected at the entrance to the Long Island Sound in wintertime when the stratification was very weak.

In the following sections, we describe the AUV and its sensors (section 2), present the methodology of our estimation technique (section 3), discuss the technique of obtaining the terms of the TKE budget (section 4), present results from data collected in two different environmental conditions (section 5), discuss these results (section 6), and summarize and present our conclusions (section 7).

2. The turbulence AUV vehicle and its sensors

The turbulence AUV (Fig. 1) performs near-synoptic microstructure and fine-structure measurements (Levine et al. 2002). It is an extended Remote Environmental Measuring Units (REMUS) vehicle (von Alt et al. 1994) that is 2.3 m long, has a diameter of 0.18 m, and weighs 560 N in air. With this first-generation vehicle, we are depth limited in boundary layer operations and to an endurance of 4 h, using rechargeable lead-acid batteries.

Onboard sensors include two CTDs, an upward- and downward-looking 1.2-MHz ADCP, and a turbulence package (two orthogonal shear probes, three accelerometers, and one FP07 fast-response thermistor). Vibration studies have led to reductions in noise transmitted to the shear probes with the use of a damping material and a probe stiffener attached to the forward end of the turbulence pressure case. Also contained in the AUV are a variety of standard REMUS "hotel sensors," including pitch, roll, heading, depth, latitude, and longitude. Measurements from the pitch and roll sensors show that the vehicle operates with mean pitch and roll angles smaller than 5° with a standard deviation of 1°. Yaw is estimated from the output of the ADCP in the form of the "bottom" track angle, and is used to estimate the angle between the centerline axis of the vehicle and water velocity and its vertical shear. Error in the yaw and heading estimates are less than 2°. In addition, the AUV navigates using a short baseline system, with onboard forward-looking and moored transponders. For safety, the AUV is tracked from a surface vessel using a Trackpoint II transponder. With these sensors, the AUV is capable of measuring the key finescale vertical gradients of velocity, temperature, salinity, and density, as well as the turbulent fluctuations of temperature and two components of the velocity that are orthogonal to the direction of AUV axis.

The wavenumber response of the shear probe and the spectral corrections at high wavenumbers follow the approach of Macoun and Lueck (2004). The FP07 fast-response thermistor has a frequency response of 25 Hz (Lueck et al. 2002). It is used to estimate heat flux but not χ, because the AUV moves too fast to fully resolve the temperature gradient spectrum, much of which comes from frequencies greater than 25 Hz. The CTD platinum thermometer is used for in situ calibration of the fast-response thermistor.

To estimate stratification, two Falmouth Scientific Instruments CTDs are mounted above and below the centerline of the AUV. The manufacturer claims accuracies of ± 0.0002 S m^{-1}, ± 0.002°C, and $\pm 0.02\%$ of full-scale pressure (100 db) for these sensors. Because of drift problems with these sensors, stratification was estimated from individual CTD vertical profiles during launch and recovery, rather than directly from the difference between the upper and lower CTDs.

To estimate the vertical gradient of finescale current shear, a modified version of the RD Instruments (RDI) 1200-kHz Workhorse navigator ADCP was integrated in the AUV hull. Upward- and downward-looking transducers share one set of electronics, and ping alternatively. The manufacturer claims accuracies for water velocities of $\pm$ 1% or $\pm$ 0.01 m s^{-1}, whichever is larger. We selected eight 0.5-m bins for both the upward and downward transducers. Because the vehicle diameter is 0.18 m, the center of the first bin is located 1.34 m from the AUV centerline.

3. Methodology

a. Multivariate probe correction

We use the acceleration measurements to minimize the contamination of the shear probe measurements by vehicular motions and vibrations of the probe mounts. A three-axis accelerometer package is mounted 0.03 m directly behind the shear probes in the turbulence pressure case. The accelerometer has the following axes: x, which is along the AUV axis and is positive forward; y, which points athwartship positive to the starboard side; and z, which is directed positive upward. The shear probe signal contamination is removed by subtracting all coherent signals from the accelerometers. Let the matrix $\mathbf{s} = \{\dot{\mathbf{v}}, \dot{\mathbf{w}}, \dot{\mathbf{T}}\}$ represent the time series of the rate of change of the transverse and the vertical velocity and temperature measured by the shear probes and the thermistor. (We use dots because the circuitry outputs the time derivative of velocity and temperature.) Further, let a_i represent the matrix of the time series of the accelerometer output with $i = 1, 2, 3$. We assume that the signals from the shear probes and the thermistor are linearly related to the true environmental turbulence plus a contribution measured by the accelerometers. That is,

$$\mathbf{s} = \hat{\mathbf{s}} + B_{ik}^{*} a_k, \tag{1}$$

where the caret (^) represents the true uncontaminated signal and the asterisk (*) represents a convolution. Repeated indices are used to imply summation; the multivariate weighting function B_{ij} represents the "transfer" of acceleration into the shear probe and thermistor signals. We also assume in (1) that vehicular motions and vibrations are statistically independent of the environmental turbulence; that is,

$$\overline{\hat{s}_i a_j} = 0$$

for all i and j. For motion with scales comparable to and longer than the length of the vehicle, this assumption breaks down because the AUV will respond to such motion. However, the correction (1) will result in an underestimate of the observed turbulent quantities $\hat{\mathbf{s}}$. The issue of body motion effects will be most germane to the estimation of the flux terms because the flux terms are sensitive to the largest measurable scales of turbulent motion. This will be examined in more detail in sections 4 and 5.

Let ϕ_i, $\hat{\phi}_i$, α_i, and β_{ij} be the Fourier transforms of s_i, $\hat{s}_i$, a_i, and B_{ij}, respectively. It follows immediately from (1) that

$$\phi_i = \hat{\phi}_i + \beta_{ik}\alpha_k. \tag{2}$$

Note that $\beta_{ij} = \beta_{ij}(f)$ is the frequency transfer function relating the probe signals to the accelerometer signals. If we multiply (2) by its complex conjugate, ensemble average, and use the fact that $\overline{\hat{s}_i a_j} = 0$, it then follows that

$$\hat{\Phi}_{ij} = \Phi_{ij} - \chi_{ik}\Gamma_{kl}^{-1}\chi_{lj}^{*}, \tag{3}$$

where $\hat{\Phi}_{ij}$ is the corrected cross-spectrum of $\hat{s}_i$,

$$\hat{\Phi}_{ij} = \langle \hat{\phi}_i \hat{\phi}_j^* \rangle \delta f;$$

Φ_{ij} is the cross-spectrum of the contaminated signal s_i,

$$\Phi_{ij} = \langle \phi_i \phi_j^* \rangle \delta f;$$

χ_{ij} is the cross-spectrum between the contaminated signal s_i, the accelerometer output, and a_j,

$$\chi_{ij} = \langle \phi_i \alpha_j^* \rangle \delta f;$$

and Γ_{ij} is the cross-spectrum of α_i,

$$\Gamma_{ij} = \langle \alpha_i \alpha_j^* \rangle \delta f.$$

In the above spectral definitions, δf is the spectral frequency (wavenumber) bandwidth of resolution. Note that the transfer function is given by

$$\beta_{ij} = \chi_{il} \Gamma_{lj}^{-1}. \tag{4}$$

Our spectral correction (3) is a multivariate version of the correction used by Levine and Lueck (1999), but uses all three accelerometer signals instead of only the unit aligned with the shear probe direction of sensitivity. If β is diagonal, then our approach reduces to that of Levine and Lueck (1999). Note that the vehicular orientation (Euler angles) does not need to be known to form this correction. The absolute orientation is established from the "hotel" pitch and roll sensors, and by yaw estimated from the ADCP bottom-track angle. We use the above technique to correct both the spectra Φ_{ij} and the time (along-track distance) series s_i of the turbulence measurements. The time series are corrected by convolving the accelerometer signals with the weighting function B_{ij}, which is obtained from the inverse Fourier transform of β_{ij} (Lueck et al. 2002; Soloviev et al. 1999).

The ensemble averages used to obtain Eq. (3) are approximated by performing a spatial average over the data. This results in some effective finite number of degrees of freedom, and thus some level of uncertainty of the corrected cross-spectral estimate given by Eq. (4). To obtain uncertainty limits of these estimates we use a procedure similar to that employed by Lueck and Wolk (1999). This is discussed in section 3b. This procedure does not invoke the Gaussian assumption, but relies on the statistics of the measurements themselves.

The largest relative contamination occurs when the environmental signals are weakest, and the multivariate technique is very effective at removing vehicular motions and vibrations from the shear probe measurements (see Fig. 2). For this Narragansett Bay example, the rate of dissipation was only 2.5×10^{-9} W kg^{-1}, and some spectrally narrow vibrational peaks were reduced

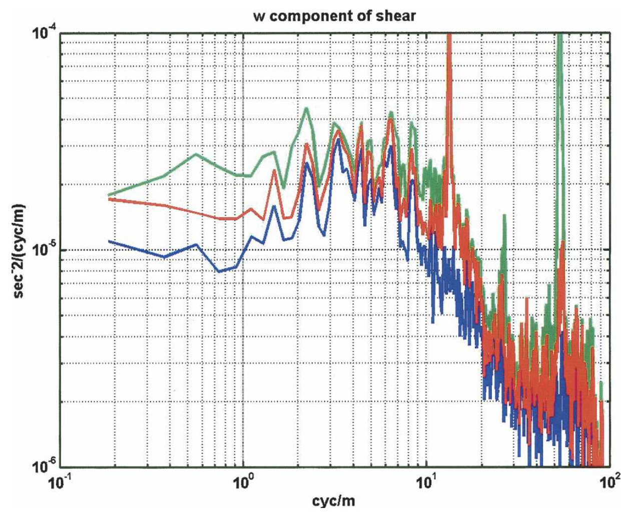

FIG. 2. Spectra of the $\dot{\mathbf{w}}'$ signal from the shear probe. The blue curve is obtained from the correction procedure of Lueck and Wolk (1999). The red curve is the procedure advanced by Levine and Lueck (1999) involving removing the component of vehicle acceleration in the same direction as the shear probe measurement. The green curve is the uncorrected spectrum. Averages are taken over twenty 50% overlapping samples.

by more than a factor of 100. In addition to removing the peak at 15 cpm, which remains untouched by the univariate approach, the multivariate approach also produces a broadband correction about 50% more than that of Levine and Lueck (1999). Note that the fully corrected spectrum (blue curve) is 2.5 times lower than the uncorrected one (green). This would reduce an estimate of the dissipation rate obtained from a fit to the "1/3 power law" by a factor of 4. Thus, for weakly turbulent environments, the correction can be very important. The combination of noise-limiting vehicle modifications, discussed previously, and the use of all of the accelerometers to remove the remaining vehicular contamination, gives us the ability to resolve dissipation rates as small as 1×10^{-9} W kg^{-1}.

In addition to correcting the high-wavenumber portion of the shear probe signals, we use (3) to correct the velocity signals derived from the shear probes at low wavenumbers to estimate the Reynolds stress. For wavenumbers smaller than 1 cpm, the correction can be significant even in regions of strong turbulence (Fig. 3), where the uncorrected value of Reynolds stress is 2.9×10^{-5} m^2 s^{-2} and the corrected value is 1.8×10^{-5} m^2 s^{-2}.

b. *Statistical significance boundaries*

Here we derive a technique for estimating the statistical significance of the corrected cospectrum of vertical

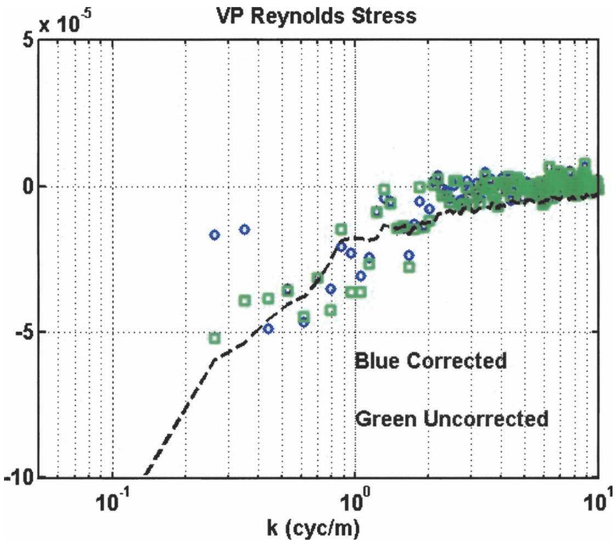

FIG. 3. Variance-preserving cospectra of the Reynolds stress term $\langle v'w' \rangle$. The blue circles are obtained from the correction procedure given by Eq. (3). The green squares are the uncorrected values. The black dashed line is the 95% confidence limit. Averages are taken over fifty 50% overlapping samples. Data are from the Long Island Sound experiment described in section 5b.

and athwartship velocity fluctuations (which give the Reynolds stress) and the corrected cospectrum of vertical velocity and temperature fluctuations (which give the vertical heat flux). We use a numerical simulation of uncorrelated data to obtain uncertainty limits. The procedure follows that employed by Lueck and Wolk (1999), and only depends on segmenting the data in time (or space, as in our case) such that the auto- and cross correlation between the segments are approximately zero, that is, there is no correlation between segments. For Gaussian random variables, this implies statistical independence. It should be noted that this, in fact, is the standard assumption used to perform spectral and cospectral estimates (Bendat and Piersol 2000).

In this work, we calculate co- and quad spectra, over a length of L, by performing an FFT on m nonoverlapping intervals. The length of each segment L/m is chosen to be longer than the auto- and cross-correlation length of the times series. To obtain the uncertainty limits for the "corrected" cross-spectral and coherence estimates, we take each dataset to be analyzed, that is, s_i, a_i, and lag one member of the pair by some integer number $p > 0$ times L/m. These lagged data are uncorrelated with the original data and with the other, unlagged, member of a pair. The expectation for the cross-spectrum and coherency is zero. However, because the data length L used for the estimation of cross-spectra is finite, our estimates will not be zero. Rather, individual estimates will distribute around zero with a distribution that depends on the length and on the statistical nature of the signals. By making many estimates of the cross-spectrum and the coherency, using different lags, we can estimate the 95% confidence for zero cross-spectra and coherency empirically without knowing the actual statistical nature of the signals. Any estimation of the cross-spectrum and the coherency of unlagged data that exceed the 95% confidence limit of zero is then statistically significant at that level of confidence. To illustrate these empirical methods, we will use the same data that were utilized to form the spectra of Fig. 2. The original time series has been doubled in length by repeating it. The doubled data series is then lagged by an interval pL/m, where $p = 2$ in this case. The coherency between the original time series and the new lagged time series is expected to be zero, but the estimated coherency is finite (Fig. 4) because of the finite number of degrees of freedom. Ninety-five percent of the coherency estimates fall below the horizontal line at 0.15 coherency; that is, there is a 95% probability that two uncorrelated signals with the length and statistical properties of our measurements will have a coherency smaller than 0.15. If we repeat this process for many different lags, we obtain consistent estimate results. The histogram of zero-coherency estimates diminishes rapidly with increasing value and is not much different from a histogram of coherency generated from Gaussian white noise. We utilize the empirical technique to calculate uncertainty limits in section 4.

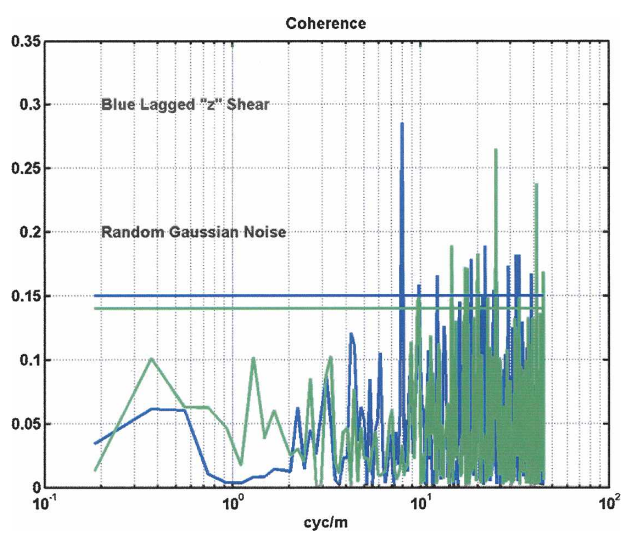

FIG. 4. The coherency of the $\dot{\mathbf{w}}$ signal from the shear probe and its lagged version with $p = 2$ (blue curve) and the coherency of a pair of Gaussian white noise signals (green curve). Ninety-five percent of the estimates fall below the horizontal lines for the actual data (blue) and the Gaussian white noise (green). Averages are taken over twenty 50% overlapping samples.

4. Estimating the terms of the turbulent kinetic energy budget

The usual starting point for estimating turbulent fluxes (Gregg 1987) is the steady-state homogeneous TKE budget equation:

$$\overbrace{-\overline{\mathbf{u}'w'}\cdot\frac{\partial\overline{\mathbf{u}}}{\partial z}}^{P} = \overbrace{-\frac{g}{\rho}\overline{\rho' w'}}^{\mathrm{B}} + \overbrace{\nu\overline{\boldsymbol{\nabla}\mathbf{u}'\cdot\boldsymbol{\nabla}\mathbf{u}'}}^{\varepsilon}, \tag{5}$$

where primes denote fluctuations, overbars represent spatial averages, and vectors are bold. Standard notation is employed for the horizontal and vertical velocity (u, w, respectively), density (ρ), temperature (T), kinematic viscosity (ν), and molecular thermal diffusivity (κ); the coordinate z is directed upward. The mean flow and mean vertical shear are entirely in the horizontal direction, and there are no mean horizontal gradients of velocity, temperature, and salinity. Term P is the Reynolds stress turbulent production term, term B is the buoyancy flux term or rate of conversion of kinetic to potential energy, and term ε is the turbulent kinetic energy dissipation rate. Typically, ε is measured and (5) is used to infer B and P (Gregg 1987) by the formulas

$$B = \Gamma\varepsilon, \tag{6a}$$

and

$$P = (\Gamma + 1)\varepsilon, \tag{6b}$$

where Γ is termed the mixing efficiency, often taken to be $\Gamma = 0.2$. Note that the assumption of stationarity and homogeneity result in the advective and transport terms in Eq. (5) being ignored. The buoyancy flux term B is positive for stably stratified flow, negative for downward convection, and zero for unstratified flow. The quantities in (5) fall into two categories—mean flow and turbulence. For measurements obtained from the AUV, the mean flow quantities are estimated by using spatial averages over the so-called finescale, which is local to but larger than the turbulence scale. The mode of operation of the vehicle and the particular environment determine the horizontal and vertical averaging distances. We use profiles of temperature and salinity and, hence, density and buoyancy frequency, obtained at the beginning of an experiment, when the AUV dived to its operational depth, and at the end of the experiment, when the AUV ascended to the surface. The turbulent quantities in the TKE budget are estimated from the turbulence package, the ADCP, and the CTD (Table 1). The correction procedure described in section 3a is used to remove body motion and probe vibration and is applied to all turbulent estimates.

TABLE 1. AUV sensors that can be used to estimate terms of the TKE budget.

	Production P	Mixing M	Dissipation ε
Sensors used	y, z shear probes 3 accelerometers ADCP	z shear probe 3 accelerometers FP07 thermistor CTD	y, z shear probes 3 accelerometers

The dissipation rate is estimated by taking the "corrected" y and z shear spectra and fitting their average to the empirical spectrum of Nasmyth (1970). A wavenumber adjustment is made for the spatial smoothing by the shear probes (Macoun and Lueck 2004).

The flux terms require the calculation of the turbulent velocity. Velocity is obtained from the shear probe data, using the approach of Wolk and Lueck (2001). They employ a scaled single-pole antiderivative lowpass filter. To accurately estimate the flux terms requires that the AUV turbulence sensors resolve the spatial scales which make significant contributions. The vehicle responds to turbulent eddies larger than its length by changing its angle of attack. Significant vehicle response occurs from turbulent eddies whose wavelengths λs are of the order of and larger than $2L$, where L is the vehicle length. The factor of 2 arises because the net effect of a turbulent eddy forcing on the vehicle must take into account the sign of the forcing. In one wavelength there are equal positive and negative contributions, and thus $\lambda/2$ is the length over which the sign of the eddy motions, on average, does not change.

The details of the vehicle response, that is, the induced displacement and rotation, are very complicated and, in addition to the nature of the perturbation field forcing, depend on factors such as the distribution of mass elements, the instantaneous lift and drag forces along the body, and the action of the horizontal and vertical control planes. See Prestero (2001) for a hydrodynamic response model of the basic REMUS vehicle. With the vehicle responding and trying to move with a surrounding larger-scale turbulent flow field, the shear probe sensors on the vehicle will underestimate the turbulent motion of the larger-scale eddies. The correction procedure described in section 3a eliminates contributions that are coherent between the accelerometers and the shear probe signals and thus removes from the shear probe signals some (if not all) of the larger-scale turbulent eddies. The result is an underestimate of the fluxes resulting from the lack of contribution of turbulence of these larger-scale eddies. That is, the finite size of the body acts as a high-pass filter at $k_C = (2L)^{-1}$ cpm on the turbulent velocity measurements. Because only one component of the Reynolds stress can be estimated by the turbulence package (because only the athwartship component y and vertical component z of turbulent shear are measured), some assumption must be made about the direction of the Reynolds stress. If we assume that the Reynolds stress and the finescale shear are aligned, that is,

$$\mathbf{s} = \frac{\boldsymbol{\tau}}{|\boldsymbol{\tau}|} = \frac{\dfrac{\partial \mathbf{u}}{\partial z}}{\left|\dfrac{\partial \mathbf{u}}{\partial z}\right|}, \tag{7}$$

where the boldface indicates a vector and $\mathbf{s}$ is a unit vector in the direction of the shear, it then follows that we have made an "eddy" viscosity assumption, namely, that

$$\boldsymbol{\tau} = \rho K_v \frac{\partial \mathbf{u}}{\partial z},$$

where

$$K_v = \frac{|\boldsymbol{\tau}|}{\rho\left|\dfrac{\partial \mathbf{u}}{\partial z}\right|}.$$

With the ADCP, we measure the vector shear ($\partial \mathbf{u}/\partial z$) and we use the shear probes to estimate the athwartship component of the Reynolds stress

$$\frac{\tau_y}{\rho} = -\overline{v'w'}.$$

The rate of production of TKE is then estimated as

$$P = \tau_s \mathbf{s} \cdot \frac{\partial \mathbf{u}}{\partial z} = -\frac{\overline{v'w'}}{\sin\psi}\left|\frac{\partial \mathbf{u}}{\partial z}\right|, \tag{8}$$

where

$$\psi = \tan^{-1}\left(\frac{\dfrac{\partial u}{\partial z}}{\dfrac{\partial v}{\partial z}}\right).$$

The buoyancy flux term B is estimated from the heat flux measurement $\langle w'T' \rangle$ by

$$B = g\left(\alpha + \beta\frac{dT}{dS}\right)\langle w'T' \rangle, \tag{9}$$

where α, β are the thermal and saline expansion coefficients and (dT/dS) is the change in temperature with salinity.

5. Observations

We will apply the estimation techniques described in sections 3 and 4 to two datasets—one obtained in a strongly stratified environment in Narragansett Bay (NB), Rhode Island, in September 2000 (Fig. 5), and second to measurements taken in weakly stratified waters off of Montauk Point on Long Island (LIS), New York, in December 2001 (Fig. 11).

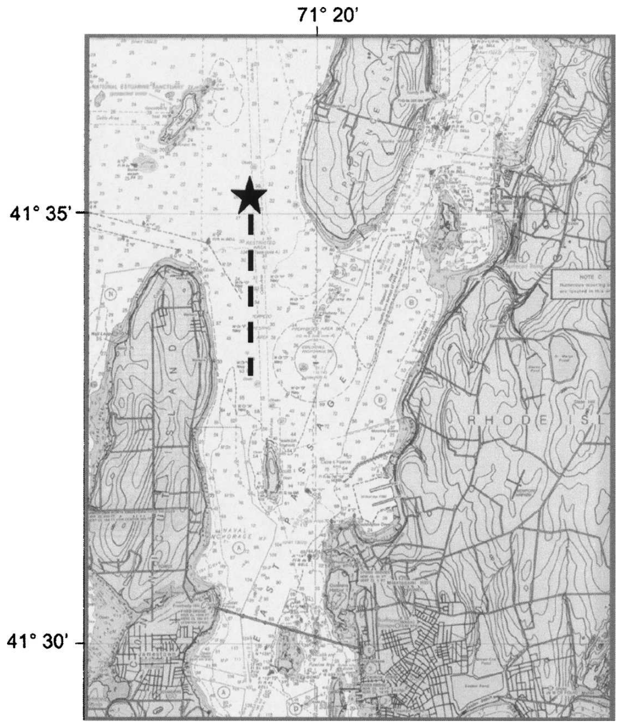

FIG. 5. Location of the Narragansett Bay experiment at 1130 eastern daylight time (EDT) 9 Sep 2000. High tide was at 1237 EDT. The star marks the starting point and the dotted line the path of the AUV. The direction of the mean current and vertical shear during the experiment was to the east.

a. *Stratified case: Narragansett Bay, September 2000*

The Narragansett Bay turbulence measurements were taken along a predominately north-to-south run at a constant depth of 8.4 m, and for a distance of 300 m. It was in a region of strong turbulence inhomogeneity. The limited amount of data and its inhomogeneity had a very strong impact on the statistical uncertainty of the estimates.

Despite the strong athwartship current to the east, the AUV maintained a steady course to the south with a typical speed of 1.4 m s^{-1} during a time of near maximum of the flood tide.

At the start of its run, the AUV descended to 10 m, rose to its operating depth of 8.4 m, and maintained that depth before rising to the surface for its recovery. The entire run lasted about 20 min. The horizontal temperature, salinity, and density gradients were fairly uniform along the track. The buoyancy frequency calculated from density profiles at the beginning and end of the run yielded $N^{-1} = 3$ min. The average magnitude of shear $|(\partial \mathbf{u}/\partial z)|$ along the run was 0.03 s^{-1}, yielding an along-track average gradient Richardson number $R_i = 1.3$.

An along-track series of turbulence data are presented in Fig. 6. Because of the decrease of turbulent intensity along the track, we divided the data into three regions, indicated by the colored double arrows. These regions are labeled I, II, and III and correspond to track distances of 810–910, 910–1010, and 1010–1130 m, respectively. In subsequent figures we retain the color convention of Fig. 6.

In Fig. 7 and Fig. 8 we show variance-preserving plots of the transverse Reynolds stress cospectrum and heat flux cospectrum, respectively. Also shown in these figures is the 95% (two sigma) confidence limit. The confidence limit is calculated by using the procedure described in section 3b. Figure 7a shows a clear trend of significant (negative) contributions beyond the 95% confidence limit for wavenumbers between 0.4 and 1.5 cpm. For Figs. 7b and 7c significant contribution appears to occur over wavenumber ranges from 0.2 to 1 cpm. Note that if contributions to the Reynolds stress cospectrum actually occur for wavenumbers less than the resolvable value of 0.2 cpm, the Reynolds stress estimate from integrating the Reynolds stress cospectrum will be an underestimate of the true value.

The heat flux cospectrum (Fig. 8) is statistically significant close to the 95% confidence limit for most of the range of wavenumbers between 0.2 and 4 cpm, with the major exception being in region I for wavenumbers between 0.7 and 1.5 cpm, where the contribution in that range of wavenumbers is close to zero. From Figs. 7 and 8 we conclude that there is sufficient statistical certainty to perform the calculation for the transverse Reynolds stress and heat flux.

In Fig. 9 the three terms of the TKE budget, namely, P, B, and ε, are shown as a function of along-track

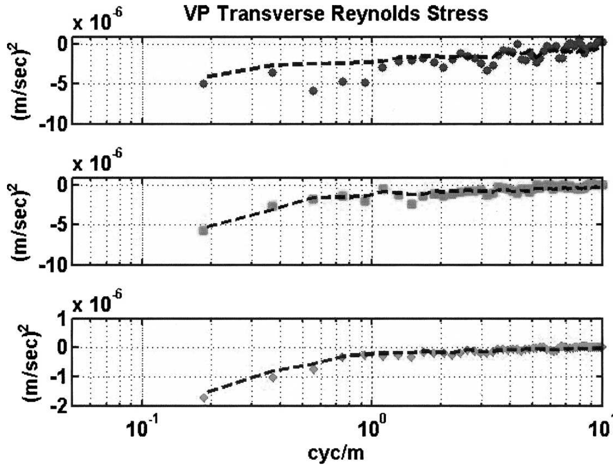

FIG. 7. The variance-preserving negative transverse (athwartship) Reynolds stress cospectrum (real part of the cross-spectrum) for the three regions of the figure. The area under the curves is the total (negative) Reynolds stress. The dashed line is the 95% confidence limits. Averages are taken over twenty 50% overlapping samples.

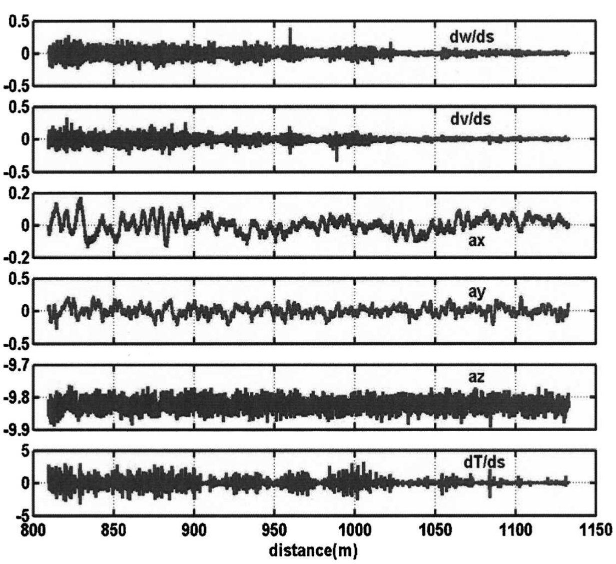

FIG. 6. Turbulence data from Narragansett Bay. The arrows are color coded to delineate three regions of stationary shear fluctuations. Distance is the along-track coordinate, to the south.

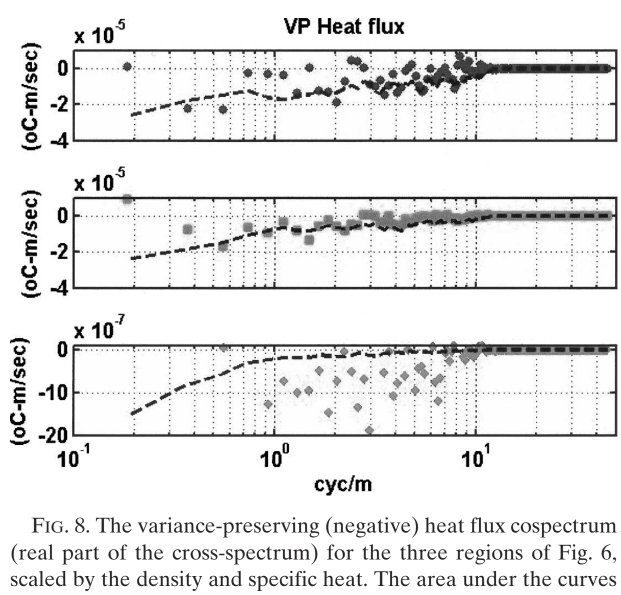

FIG. 8. The variance-preserving (negative) heat flux cospectrum (real part of the cross-spectrum) for the three regions of Fig. 6, scaled by the density and specific heat. The area under the curves is the total heat flux. The dashed line is the 95% confidence limits. Averages are taken over twenty 50% overlapping samples.

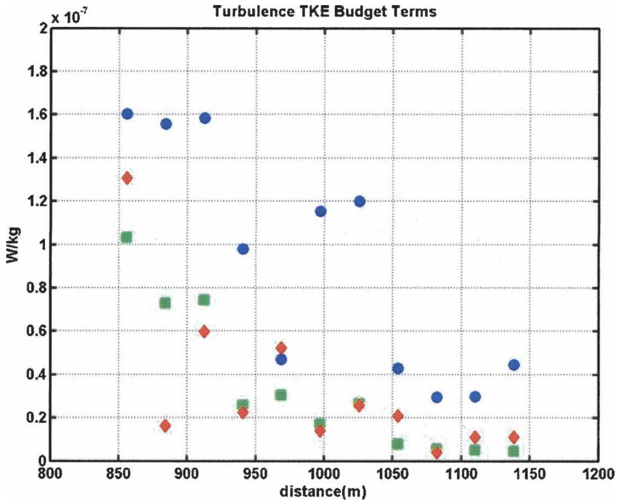

FIG. 9. The terms of the TKE budget [Eq. (1)] P, M, and ε are plotted vs the AUV along-track distance. Blue is the production term P, red is the mixing term M, and green is the dissipation rate ε.

distance. The fractional imbalance of the TKE budget, defined as

$$\Delta = 2\frac{P - B - \varepsilon}{|P| + |B + \varepsilon|}, \tag{10}$$

fluctuates about 0 with a mean of 0.2 from the initial distance of $x = 800$ m to $x = 920$ m. Farther down the track, the estimate of production is consistently larger than the sum of the buoyancy flux and the rate of dissipation. The fractional imbalance Δ in this region is approximately 0.8. In Fig. 10 we present the buoyancy Reynolds number,

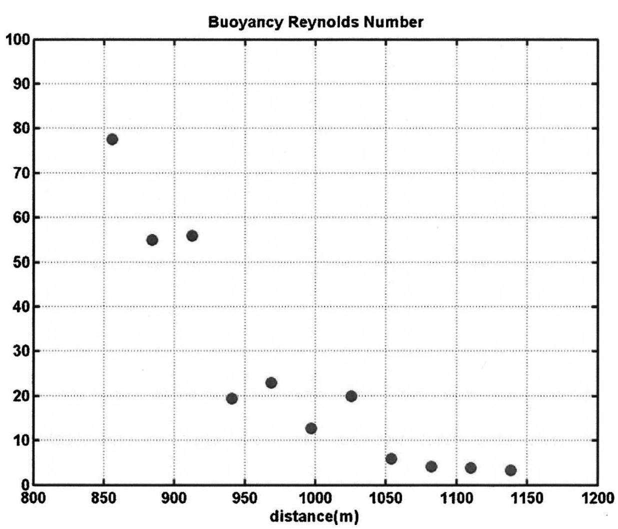

FIG. 10. Buoyancy Reynolds number R_B vs along-track distance.

$$R_B = \frac{\varepsilon}{\nu N^2}, \tag{11}$$

as a function of along-track distance. As ε decreases, R_B decreases along the track. Note that R_B falls below 20 beyond $x = 920$ m. The value of $R_B = 20$ has been identified as a critical value below which the turbulence ceases to be isotropic and active, and is expected to be highly damped (Itsweire et al. 1986). Note that for $x >$ 920 the TKE budget does not close. Because turbulence in this range is far from an active isotropic classical form, it is not unexpected that the TKE budget would not close in that regime.

b. *Weakly stratified case: Long Island Sound, December 2001*

The second case that we examine is a 1600-m-long run taken in weakly stratified waters off Montauk Point in December of 2001 (Fig. 11). The AUV followed a 1° "yo–yo" path and repeatedly cycled between depths of 3 and 6 m. The direction of travel was nearly north–south. This region has many coastal frontal features, including a shelf front, a headland front, a river plume front, and a tidal mixing front (Bowman and Esaias 1991).

The data were collected during the FRONT experiment, and a December 2001 frontal-scale survey showed relatively salty, warm water offshore with a density increase of approximately 0.3 kg m^3 over a distance of 10 km in the seaward direction. The temperature, salinity, and density show very little variation with changes in AUV depth. However, the salinity decreases by 0.15 psu along the first two-thirds of the track, and then the salinity and temperature increased slightly for

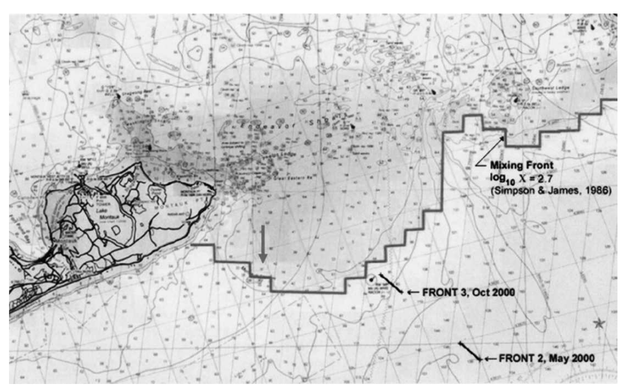

FIG. 11. Site of the Long Island Sound December 2001 experiment. The tidal mixing front in green is predicted by the Massachusetts Institute of Technology (MIT) GCM model (Levine et al. 2002).

the reminder of the course. The initial descent showed very little vertical stratification, but the final ascent showed a colder and fresher layer above 2.5-m depth below which there was a stable density gradient with $N^{-1} = 10$ min.

Because of the close proximity of the AUV to the sea surface, only the downward-directed ADCP provides good data. The shear is estimated from the mean gradient over the first eight (0.5-m interval) bins, which is then averaged over four pings spanning 34 m along the track. The track is initially almost aligned with the prevailing current, but, after a 500-m distance, the angle between the track and the current exceeded 25°. Reasonable (defined using the significance levels developed in section 3b) estimates of the total stress using the transverse component of Reynolds stress and vehicle orientation angle are then possible for along-track distances greater than 500 m using Eq. (8).

The shear in the down-current direction is of the order of 0.01 s^{-1} and increases in magnitude along the track. The crosscurrent shear fluctuates as much as the down-current shear, but its magnitude is much smaller and there is no significant trend along the track of the AUV. We will ignore the crosscurrent shear and assume that the local shear is aligned in the direction of the current vector; this smoothes the estimate of the shear direction. Analysis of the ADCP shear data indicates that the statistical uncertainty of the current direction is much less than the uncertainty of the shear direction. Because the vehicle cycles between 3- and 6-m depths, there is a slight mismatch between the depth of the shear estimates and that of the turbulent estimates. However, from the structure of the larger-scale flow field (ODH04), and from the temperature, salinity, and density profiles observed by the vehicle on descent and ascent, we expect that the shear below the AUV will give a reasonable estimate of the shear along the centerline of the AUV.

The variance of microstructure shear is large and fairly homogenous along the track of the AUV (Figs. 12 a,b,c). Note that the turbulent shear values in Figs. 12a and 12b are an order of magnitude larger than in the Narragansett Bay values (Figs. 6a,b).

In Figs. 13 and 14 we present the variance-preserving cospectrum of the transverse Reynolds stress and heat flux, respectively. Averages are taken over fifty, 50% overlapping samples. Note that Fig. 14 shows positive contributions, in contrast to those in Fig. 8, for the stratified Narragansett Bay case. Figure 14 thus indicates a downward convection of heat.

Figures 13 and 14 show statistically significant contributions over a finite well-resolved wavenumber bandwidth. For the case of the transverse Reynolds stress that range is 0.4–1.8 cpm, while for the heat flux that range is 0.25–0.7 cpm.

Figure 15 shows two terms of the TKE budget P and ε calculated as discussed in section 3. In general, these values are quite large, of the order of several times 10^{-6} W kg^{-1}. Using Eq. (9) in the integral of the heat flux spectrum shown in Fig. 14 results in a value of B of the order of 10^{-8} W kg^{-1}, which is two orders of magnitude smaller than P and ε. Thus, the buoyancy term B does not contribute significantly to the TKE budget balance and is not included in the TKE budget (Fig. 15). Although there apparently was significant surface cooling (estimated to be 300 W m^{-2}) because of the salt

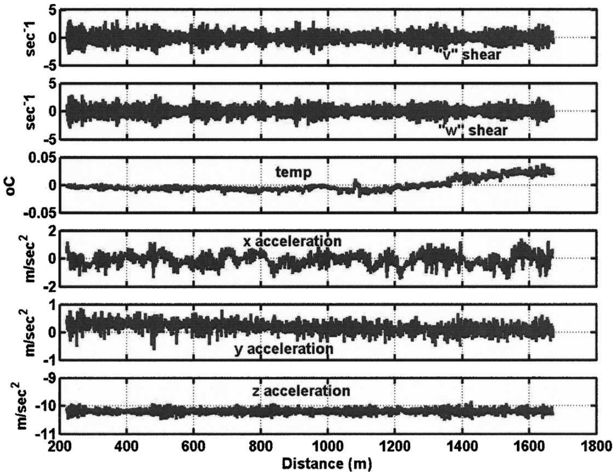

FIG. 12. Turbulence data from December 2001 Long Island Sound experiment.

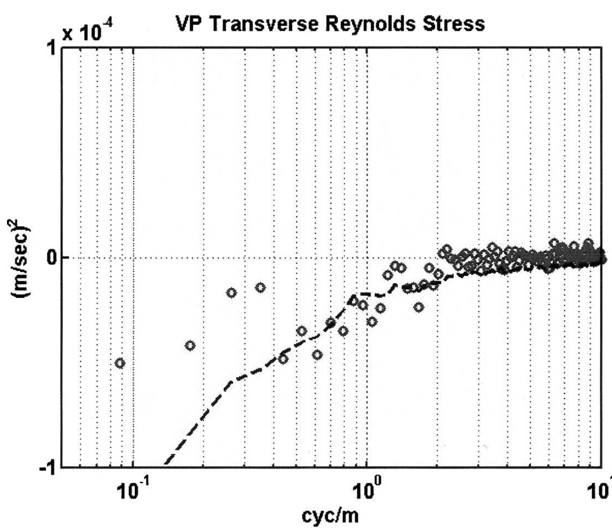

FIG. 13. The negative athwart ship Reynolds stress cospectrum. The dashed line is the 95% confidence limit. The black dashed line is the 95% confidence limit. Averages are taken over fifty 50% overlapping samples.

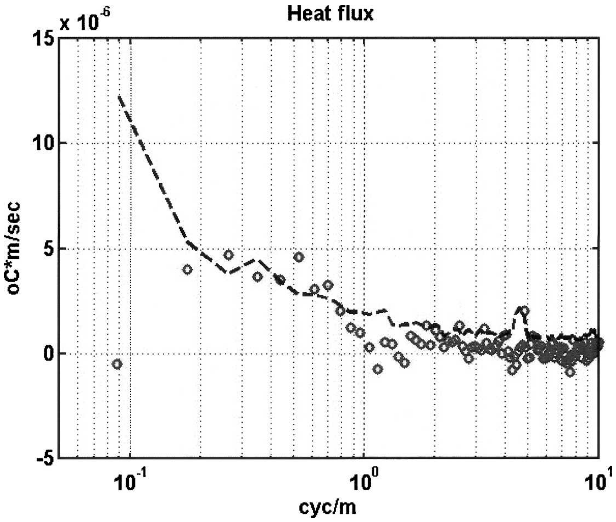

FIG. 14. The heat flux cospectrum. The dashed line is the 95% confidence limits.

stratification below the surface layer, only a small portion of the vertical heat flux cooling (of the order of 30 W m^{-2}) extended to the depth of the AUV operation. Note that the surface heat flux of 300 W m^{-2} would still produce a buoyancy flux B of one order of magnitude smaller than the values of P and ε of Fig. 15. Thus, we conclude that turbulence during this AUV run was generated by the action of the local shear and not downward advective cooling, and it is expected that only the P and ε terms would be significant in the TKE budget.

From Fig. 15 the turbulent production term and the turbulent dissipation term track very well with each other. Note that at 800- and 1200-m distances both show approximately the same increase in magnitude. However, the production term shows considerably more scatter. This can be seen more clearly in Fig. 16, where we show the probability distributions of the logarithm of these two terms along with that of the transverse Reynolds stress. Note that the rate of dissipation has a near-lognormal distribution with a fairly narrow variance (Fig. 16c). On the other hand, the distribution of the rate of production is much wider and is possibly not lognormal (Fig. 16b). This difference in the variance of the distributions of P and ε is because of the effective number of degrees of freedom in the calculation for each of these quantities. The dissipation rate occurs at the smallest scales of the turbulence and, therefore, the 36-m-long estimates used to calculate each of the ε estimates in Fig. 15 have many degrees of freedom. The production term P arises from a contribution at the largest scales of the turbulence and so this estimate has a considerably smaller number of degrees of freedom than each ε estimate. The rate of production of TKE and its rate of dissipation have a correlation coefficient of 0.38, with a probability of 97% that this correlation is not the result of random chance. The bias toward larger values of the production term versus the dissipation term can be attributed to the differences in their probability distributions, as shown in Fig. 16.

6. Discussion

Because the AUV responds to turbulent eddies of wavelengths longer than approximately twice the length of the vehicle ($\lambda = 2L = 4.6$ m), the turbulent

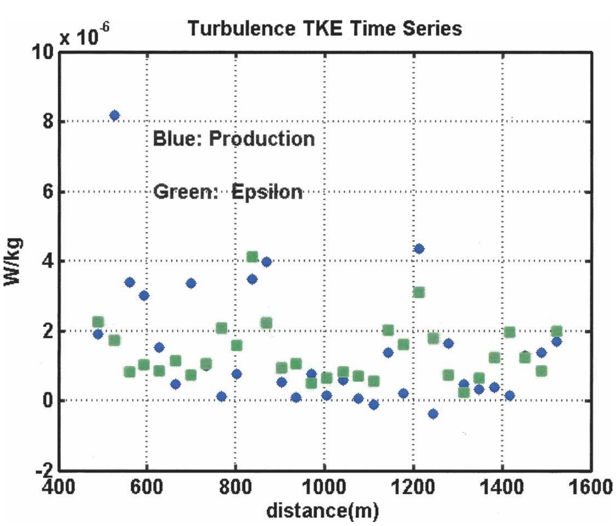

FIG. 15. The two major terms of the TKE budget as a function of along-track distance. Each point is averaged over 36 m.

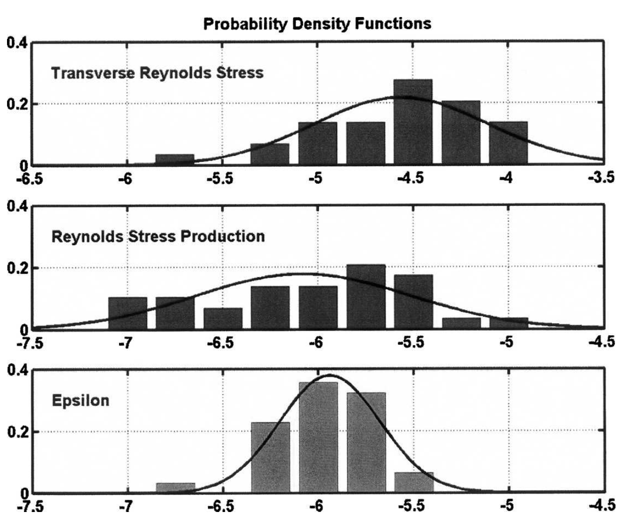

FIG. 16. The probability density for the base-10 logarithm of athwartship (a) Reynolds stress, (b) the rate of TKE production, and (c) its rate of dissipation.

sensors on the AUV will not be able to resolve these larger scales of motion. This would lead, in general, to an underestimate of the fluxes. Thus, it is important to estimate the dominant length scales that contribute to the flux terms, that is, momentum flux and heat flux. For unstratified flow this spatial scale is expected to be of the order of the energy-containing scale l (Tennekes and Lumley 1972), where

$$l = 2\pi\left[\frac{\varepsilon}{\left(\dfrac{du}{dz}\right)^3}\right]^{1/2}. \tag{12}$$

For the case of stratified flow, the appropriate length employed to estimate the magnitude of the largest scale of the eddies is the Ozmidov length scale

$$L_O = 2\pi\left(\frac{\varepsilon}{N^3}\right)^{1/2}. \tag{13}$$

Our direct and fully resolved measurement of the dissipation rate and the measurement of background shear and buoyancy frequency allow us to estimate (12) and (13). In Figs. 17 and 18, we show a plot of the TKE budget fractional imbalance parameter Δ given by Eq. (10) and a plot of the length scale L_O for the Narragansett Bay data (Fig. 17b) and l for the Long Island Sound data (Fig. 18b).

For the strongly stratified environment in Narragansett Bay, Fig. 17 shows that the Ozmidov scale is always significantly shorter than $2L = 4.6$ m. There does appear to be a slight decrease in the magnitude of L_O with along-track distance. The region of relatively low TKE fractional imbalance $x < 920$ m is the region of larger values of L_O. As discussed in section 4b for along-track ranges greater than $x = 920$ m where the fractional imbalance approaches 1, values of R_B (Fig. 10) fall below the critical value of 20, where laboratory observations suggest that active turbulence ceases to exist. We can conclude from this that the TKE budget approximately closes in the regime where active turbulence is expected, $x < 920$ m corresponding to $R_B > 20$.

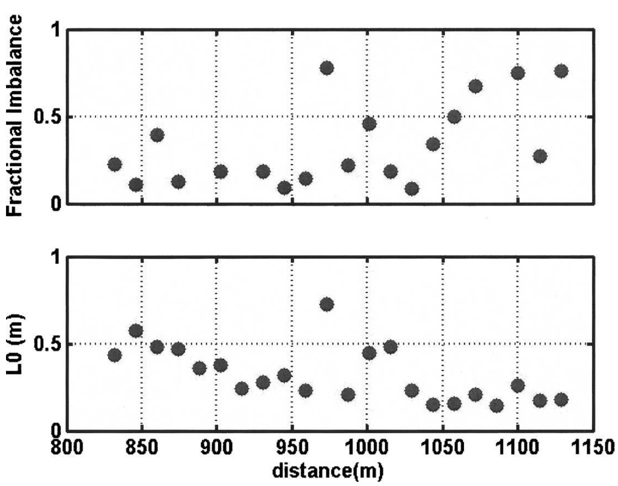

FIG. 17. NB case: (a) the along-track plot of TKE fractional imbalance Δ [Eq. (10)] vs along-track distance, and (b) the along-track plot of the Ozmidov scale L_O.

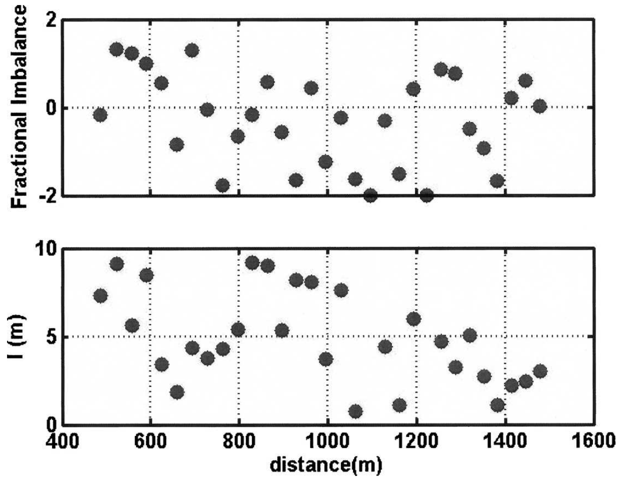

FIG. 18. LIS case: (a) the along-track plot of TKE fractional imbalance Δ [Eq. (10)] vs along-track distance (For this case, the buoyancy flux term B is negligible), and (b) the along-track plot of turbulent energy-containing scale l.

For the unstratified LIS case from Fig. 18, both the fractional imbalance (Fig. 18a) and the eddy-containing scale l vary. The mean of the fractional imbalance is

$$\langle\Delta\rangle = -0.29,$$

with an rms variance of

$$\langle\Delta'^2\rangle^{1/2} = 1;$$

while the mean of the energy-containing eddy length scale is

$$\langle l\rangle = 4.8 \text{ m},$$

with an rms variance of

$$\langle(l')^2\rangle^{1/2} = 2.6 \text{ m}.$$

Thus, the length scale l is comparable to the response wavelength of the AUV ($2L = 4.6$ m), and the estimated Reynolds stress may have at times been underestimated. This supports the result that the mean of the fractional imbalance is slightly negative, implying that on average the production term was somewhat smaller than the dissipation term. One other factor that must be taken into account in interpreting these results is that the TKE budget [Eq. (5)] involves neglecting the turbulent transport terms. The order of magnitude estimates of these terms (Tennekes and Lumley 1972) shows that such terms are in fact comparable to P and ε. They become zero when the assumption of homogeneity and stationarity is invoked. Thus, the value of the (spatial) averaging scale is very important in assessing the validity of the TKE budget. For an averaging distance of the entire track of the AUV (1.6 km), the TKE budget for the LIS case is well satisfied with a slight underestimate of the production term resulting from the marginal resolution of the largest scale of motion. However, on a scale of averaging of 34 m, the TKE budget is not satisfied.

7. Summary and conclusions

In this article we develop techniques to use standard micro- and fine-structure sensors on board a small AUV to obtain the terms of the steady-state TKE budget. The turbulence REMUS vehicle is equipped with two CTDs, an upward- and downward-looking 1.2-MHz ADCP, and a thrust probe turbulent shear package (Lueck et al. 2002). With these instruments both the fine-scale shear and buoyancy field, as well as the microscale transverse velocity, can be estimated. In Table 1 we show how the AUV turbulence and fine-scale sensors can be used to obtain the terms of the steady-state TKE budget [Eq. (5)]. To minimize the effect of probe vibration and vehicle motion on turbulent velocity and shear estimates, we have extended the one component coherent subtraction technique of Levine and Lueck (1999) to include all three components of vehicle/probe motion. This results in improved estimates of the terms of the TKE budget, ε, P, and B. A statistical procedure for estimating uncertainly limits for the corrected flux cospectra of momentum and heat is also developed.

Calculation of the heat flux occurs directly from integrating the corrected turbulent vertical velocity data and correlating it with the corrected fast-response temperature data. However, only one vector component of the vector Reynolds stress can be estimated by an analogous procedure. This results because the thrust probes only respond to forces perpendicular to the direction of motion of the vehicle. Note that, unlike vertical microstructure profilers, a horizontal profiling platform such as an AUV or a towed vehicle (Lueck et al. 2002), equipped with a thrust probe whose axis is in the horizontal direction, can be used to estimate vertical velocity. To obtain the component of Reynolds stress in the direction of vehicle motion, a generalized eddy viscosity formulation is invoked. This is equivalent to assuming that the Reynolds stress vector is aligned in the direction of the mean shear vector. The later can be measured by the vehicle ADCP.

Using these techniques the TKE budget terms for two datasets from very different environments are obtained. For both datasets it is observed that the flux estimates have a wide wavenumber range of statistically significant values. The issue then to be resolved is how well the estimates can resolve the largest scales of turbulent motion. For the strongly stratified case discussed in section 5a, the Ozmidov scale is much smaller than the vehicle response scale ($2L = 4.6$ m), and the calculations of Reynolds stress and heat (buoyancy) flux appear to be well resolved. The TKE budget closes reasonably well over the region of turbulence expected to be active, $R_B > 20$. For $R_B < 20$, experimental results suggest that turbulence does not exist, or that the type of turbulence that exists in that regime is far from classical turbulence (Itsweire et al. 1986). In this regime it is not unexpected that the TKE budget would not close.

For the case of Long Island Sound, on average over the range of 1.6 km, the production term P nearly balances ε. The buoyancy term B was found to be two orders of magnitude smaller than the other terms. There is a slight negative bias in the TKE imbalance parameter Δ, which does indicate a slight underestimate on average of the production term. This agrees with the estimated value of the energy-containing eddy scale of 4.8 m, which is of the order of the vehicle response scale $2L = 4.6$ m. It is also noted that the production term P and the dissipation rate term ε both exhibit significant scatter for the spatial averages used in the TKE budget calculations (Fig. 15), and that over that scale the TKE budget does not balance. It is suggested that this imbalance is because of the small number of effective degrees of freedom in calculating each value of P. If we take l to be of the order of 5 m, then there are only seven effective degrees of freedom in this estimate. Moreover, the turbulent transport term is of the same order of magnitude as the production and dissipation term in Eq. (5), and is neglected only with the assumption of stationarity and homogeneity. Thus, the choice of averaging distance (time) plays a very important role in applying the concept of TKE budget closure.

Acknowledgments. This work was supported by ONR under Grants N00014-04-01-0254, N0014-03-1-0380, N00014-02-1-0684, N00014-01-WX-2-0577, NUWC ILIR (ERL), and N00014-03-1-0616 (RGL). The authors thank an anonymous reviewer for valuable comments and suggestions for the derivation presented in section 3a for the multivariate correction procedure.

REFERENCES

Bendat, J. S., and A. G. Piersol, 2000: *Random Data: Analysis and Measurement Procedures*. Wiley-Interscience, 594 pp.

Bowman, M. J., and W. E. Esaias, 1991: Fronts, stratification, and mixing in Long Island and Block Island Sounds. *J. Geophys. Res.,* **86,** 4260–4264.

Caldwell, D. R., and J. N. Moum, 1995: Turbulence and mixing in the ocean. *Rev. Geophys.,* **33** (Suppl.), 1385–1394.

Cox, C., Y. Nagata, and T. Osborn, 1969: Oceanic fine structure and internal waves. *Bull. Japan. Soc. Fish. Oceanogr.*, Special Issue: Prof. Uda's Commemorative Papers, 67–71.

Fleury, M., and R. G. Lueck, 1992: Microstructure in and around a double-diffusive interface. *J. Phys. Oceanogr.,* **22,** 701–718.

——, and ——, 1994: Direct heat flux measurements using a towed vehicle. *J. Phys. Oceanogr.,* **24,** 701–718.

Gargett, A. E., 1982: Turbulence measurements from a submersible. *Deep-Sea Res.,* **29,** 1141–1158.

——, 1989: Ocean turbulence. *Annu. Rev. Fluid Mech.,* **21,** 419–451.

Gregg, M. C., 1987: Diapycnal mixing in the thermocline: A review. *J. Geophys. Res.,* **92,** 5249–5284.

——, W. C. Holland, E. E. Aagaard, and D. H. Hirt, 1982: Use of a fiber optic cable with a free-fall microstructure profiler. *IEEE/MTS Ocean '82 Conf. Proc.*, Vol. 14, IEEE/MTS, 260–265.

Itsweire, E. C., K. N. Helland, and C. W. Von Atta, 1986: The evolution of grid-generated turbulence in a stably stratified fluid. *J. Fluid Mech.,* **162,** 299–338.

Ivy, G. N., J. Imberger, and J. R. Koseff, 1998: Buoyancy fluxes in a stratified fluid. *Physical Processes in Lakes and Oceans*, J. Imberger, Ed., *Coastal and Estuarine Series*, Vol. 54, Amer. Geophys. Union, 377–388.

Levine, E. R., and R. G. Lueck, 1999: Turbulence measurements from an autonomous underwater vehicle. *J. Atmos. Oceanic Technol.,* **16,** 1533–1544.

——, ——, R. R. Shell, and P. Licis, 2000: Coastal turbulence estimates in ocean modeling and observational studies near LEO-15. *Eos, Trans. Amer. Geophys. Union*, **80,** 49.

——, L. Goodman, R. Lueck, and C. Edwards, 2002: Balancing turbulent energy budgets and model verification with AUV-based sampling in the FRONT coastal front. *Eos, Trans. Amer. Geophys. Union*, **83,** 4.

Lueck, R. G., and F. Wolk, 1999: An efficient method for obtaining the significance of covariance estimates. *J. Atmos. Oceanic Technol.,* **16,** 773–775.

——, ——, and H. Yamazaki, 2002: Oceanic velocity measurements in the 20th Century. *J. Oceanogr.,* **58,** 153–174.

Macoun, P., and R. Lueck, 2004: Modeling the spatial response of the airfoil shear probe using different sized probes. *J. Atmos. Oceanic Technol.,* **21,** 284–297.

Moum, J. N., 1990: The quest for K_ρ—Preliminary results from direct measurements of turbulent fluxes in the ocean. *J. Phys. Oceanogr.,* **20,** 1980–1984.

Nasmyth, P. V., 1970: Ocean turbulence. Ph.D. thesis, University of British Columbia, 69 pp.

Osborn, T. R., 1974: Vertical profiling of velocity microstructure. *J. Phys. Oceanogr.,* **4,** 109–115.

——, 1980: Estimates of the local rate of vertical diffusion from dissipation measurements. *J. Phys. Oceanogr.,* **10,** 83–89.

——, and R. G. Lueck, 1985: Turbulence measurements from a submarine. *J. Phys. Oceanogr.,* **15,** 1502–1520.

Prestero, T., 2001: Verification of a six-degree of freedom simulation model for the REMUS Autonomous Underwater Vehicle. M.S. thesis, MIT/WHOI, 128 pp.

Soloviev, A., R. Lukas, P. Hacker, H. Schoeberlein, M. Backer and A. Arjannikov, 1999: A near-surface microstructure sensor system used during TOGA COARE. Part II: Turbulence measurements. *J. Atmos. Oceanic Technol.,* **16,** 1598–1618.

Stillinger, D. C., K. N. Helland, and C. W. Van Atta, 1983: Experiments on the transition to homogeneous turbulence to internal waves in a stratified fluid. *J. Fluid Mech.,* **131,** 91–122.

Tennekes, H., and J. Lumley, 1972: *A First Course in Turbulence*. MIT Press, 300 pp.

von Alt, C. J., B. Allen, C. Austin, and R. Stokey, 1994: Remote Environmental Measuring Units. *Proc. Autonomous Underwater Vehicle Conf. '94*, Cambridge, MA, 13–19.

Wolk, F., and R. G. Lueck, 2001: Heat flux and mixing efficiency in the surface mixed layer. *J. Geophys. Res.,* **106,** 19 547–19 562.

Yamazaki, H., R. Lueck, and T. Osborn, 1990: A comparison of turbulence data from a submarine and a vertical profiler. *J. Phys. Oceanogr.,* **20,** 1778–1786.